Available online at www.sciencedirect.com
SCIENCE DIRECT®
Journal of Power Sources 137 (2004) 80–87
JOURNAL OF POWER SOURCES
www.elsevier.com/locate/jpowsour

Influence of cointercalated HF on the electrochemical behavior of highly fluorinated graphite

Tsuyoshi Nakajima [a,*], Vinay Gupta [a], Yoshimi Ohzawa [a], Henri Groult [b], Zoran Mazej [c], Boris Žemva [c]

[a] *Department of Applied Chemistry, Aichi Institute of Technology, Yakusa-cho, Toyota-shi 470-0392, Japan*
[b] *Laboratoire Liquides Ioniques & Interfaces Chargées, Université Pierre et Marie Curie, CNRS UMR7612, 4 Place Jussieu, 75252 Paris Cedex 05, France*
[c] *Jožef Stefan Institute, Jamova 39, 1000 Ljubljana, Slovenia*

Received 13 April 2004; received in revised form 21 May 2004; accepted 21 May 2004
Available online 8 July 2004

Abstract

Highly fluorinated graphite was prepared at room temperature using high oxidation state transition metal complex fluoride (K_2PdF_6, K_2MnF_6, K_2NiF_6 or $KAgF_4$) and elemental fluorine under pressure ((5.9–11.8) $\times 10^5$ Pa) in anhydrous liquid HF (aHF). The composition of the fluorinated graphite samples ranged from $C_{1.1}F$ to $C_{1.9}F$ containing small amounts of HF. IR absorption spectra revealed that stage 1 phase of C_xF contained several different phases with planar (sp^2) and puckered (sp^3) graphene layers. Electrochemical discharge of the fluorinated graphite showed that profile of discharge potential and discharge capacity varied depending on the amount of cointercalated HF. The C_xF samples with less amounts of HF and $HF_2^{\delta-}$ had relatively flat discharge potentials and large discharge capacities. The discharge capacity reached 500–600 mAh/g in 1 mol/dm^3 $LiClO_4$–propylene carbonate solution at 25 °C. Chemical diffusion coefficients of Li^+ ion in the intermediate discharge products were (4.4–13) $\times 10^{-12}$ cm^2/s from impedance measurement.

Keywords: Fluorination; Fluorinated graphite; Graphite intercalation compound; Primary lithium battery

1. Introduction

Reaction of graphite with elemental fluorine yields two kinds of intercalation compounds of graphite: graphite fluorides $(CF)_n$ and $(C_2F)_n$, and fluorine–graphite intercalation compound, C_xF [1,2]. Graphite fluorides with puckered (sp^3) graphene layers to which fluorine atoms are covalently bonded are synthesized by fluorination of carbon materials such as natural graphite, synthetic graphite and petroleum coke at high temperatures of 300–600 °C. $(CF)_n$ is prepared from various kinds of carbon materials, for example, by fluorination of petroleum coke at 300–600 °C or fluorination of graphite at ca. 600 °C. $(C_2F)_n$ is formed from high crystalline graphite in a limited temperature range of 350–400 °C. Fluorination of graphite between 400 °C and ca. 550 °C provides a mixture of $(CF)_n$ and $(C_2F)_n$. In a low temperature range less than about 100 °C, fluorine–graphite intercalation compound, C_xF is obtained by the fluorination of graphite in the presence of a Lewis acid such as HF, having planar (sp^2) graphene layers with ionic or semi-ionic (semi-covalent) C–F bond [1,2]. Fluorination of graphite is usually made in a fluorine atmosphere in the presence of Lewis acid(s) or in anhydrous liquid HF (aHF) with elemental fluorine [1,2]. The synthesis of C_xF in aHF with fluorine gas yields stage 1 compound, the composition of which reaches C_2F [3–7]. The use of gaseous HF and IF_5 with elemental fluorine also produced C_xF with approximate composition of C_2F [8–11]. Fluorination of graphite by high oxidation state transition metal fluoride such as AgF_3 or NiF_3 and elemental fluorine produced stages 1–4, $C_{4.2}F$–$C_{14.6}F$ [12]. High oxidation state transition metal complex fluoride was employed for the fluorination of graphite in aHF, which gives stage 1 C_xF with by-products insoluble in aHF [13]. Highly fluorinated graphite was obtained by the fluorination using high oxidation state transition metal complex fluoride and elemental fluorine under pressure in aHF at room temperature [14,15]. Electrochemical discharge behavior of graphite fluoride and C_xF are different from each other due to the difference in C–F bonds and fluorine contents. C_xF gives a higher discharge potential

* Corresponding author. Tel.: +81 565 48 8121x2201; fax: +81 565 48 0076.
E-mail address: nakajima-san@aitech.ac.jp (T. Nakajima).

0378-7753/$ – see front matter © 2004 Elsevier B.V. All rights reserved.
doi:10.1016/j.jpowsour.2004.05.042

than graphite fluoride because of the higher activity of fluorine in C_xF with semi-ionic C–F bond than that of graphite fluoride with covalent C–F bond [1,2,8–11,14,16,17]. However, C_xF usually has a smaller discharge capacity than graphite fluoride $(CF)_n$ due to the lower fluorine content and longer diffusion path of Li^+ ion in C_xF [14]. When C_xF is synthesized in aHF, some amount of HF is cointercalated into graphite because the fluorination reaction proceeds via C_xHF_2, which is formed at the beginning of fluorination of graphite in aHF (Eq. (1), step 1). Mobile $HF_2{}^{\delta-}$ easily diffuses into graphite and HF is gradually desolvated along with formation of semi-ionic C–F bond at stage 1 (Eq. (1), step 2). Cointercalated HF thus remains in graphene layers after the semi-ionic C–F bond is formed. HF remaining in graphite must be removed from the product by pumping, however, complete removal of HF is usually difficult (Eq. (2)). Stage 1 C_xF sometimes contains stage 2 and 3 phases as minor components, in which C–F bond is nearly ionic and main intercalated species are $HF_2{}^{\delta-}$ [1,2].

$$xC + \frac{1}{2}F_2 + yHF \rightarrow C_xHF_2(HF)_{(y-1)} \rightarrow C_xF(HF)_y \quad (1)$$

$$C_xF(HF)_y \rightarrow C_xF(HF)_z + (y-z)HF \quad \text{(by pumping)} \quad (2)$$

In the present study, highly fluorinated graphite samples were prepared at room temperature in aHF using high oxidation state transition metal complex fluoride and elemental fluorine under pressure, and their structure and electrochemical discharge behavior were investigated.

2. Experimental

2.1. Synthesis of highly fluorinated graphite, C_xF

Starting material was Madagascar natural graphite powder (57–74 μm, 99.4%). K_2MnF_6 and K_2PdF_6 were prepared as described in Refs. [18,19], respectively. Highly fluorinated graphite was prepared in aHF using elemental fluorine under pressure ($(5.9-11.8)\times10^5$ Pa) and high oxidation state transition metal complex fluorides (K_2PdF_6, K_2MnF_6, K_2NiF_6, $KAgF_4$). The fluorination of graphite was performed at room temperature for 2–3 weeks using FEP (tetrafluoroethylene-hexafluoropropylene copolymer) or PFA (tetrafluoroethylene-perfluoro-alkylvinylether copolymer) reaction vessels. The details of the preparation procedure of C_xF using K_2NiF_6 or $KAgF_4$ are described elsewhere [14]. In the case of K_2MnF_6 and K_2PdF_6, a slightly modified procedure was used. A reaction mixture of graphite powder, high oxidation state complex fluoride, elemental fluorine and aHF was exposed to ultra-violet (UV) light all the time during the synthesis in order to oxidize possible lower Mn or Pd binary and ternary fluorides back to tetravalent state. After 3–4 weeks, the reaction was stopped and K_2MF_6 (M = Mn, Pd) was washed away by several repetitions of dissolving and decanting it. Obtained C_xF samples were in most cases contaminated with traces of M^{2+} and/or M^{3+} by-products insoluble in aHF. After adding about 100 mg of KF, fresh aHF and elemental fluorine (2×10^5 Pa) to highly fluorinated graphite and exposing it to UV light for 2 days, M^{2+} and/or M^{3+} by-products were washed away as K_2MF_6 together with an excess of KF in a form of yellow solution. The prepared C_xF samples were dried by pumping for ~6 weeks at room temperature.

2.2. Analyses of the products

The C_xF samples obtained were analyzed by elemental analysis, X-ray powder diffractometry and IR absorption spectroscopy using KBr method. Elemental analysis of C, H and F were made at Elemental Analysis Center of Faculty of Pharmaceutical Science of Kyoto University.

The electrochemical reduction was performed using a three-electrode cell at 25 °C in a glove box filled with argon. Preparation of a working electrode was the same as described in a previous paper [20]. The counter and reference electrodes were metallic lithium and electrolyte solution was 1 mol/dm^3 $LiClO_4$–propylene carbonate (PC). The galvanostatic discharge of C_xF was made at a current density of 10, 35 or 40 mA/g.

The kinetic characteristics for lithium insertion into C_xF were obtained from impedance measurements. Firstly, a galvanostatic pulse was applied to the electrode for a sufficient time to reach a constant discharge potential called closed circuit voltage (CCV), which corresponds to a discharge ratio, y. Secondly, the current was interrupted. The electrode tended gradually towards equilibrium, which gives an equilibrium potential called open circuit voltage (OCV). At this potential corresponding to the discharge ratio, y, the impedance measurement was performed. After that, next measurement was done in the same manner and repeated totally 5 or 6 times at different discharge ratios [21,22]. The frequency range was 10^5 to 10^{-3} Hz and the amplitude of the sinusoidal signal was 10 mV peak-to-peak. The OCV was measured after 24 h when the potential shift was stabilized to less than 0.2 mV/h. The impedance experiments were performed using a Radiometer Copenhagen *Volta*Lab^{TM}40 generator.

3. Results and discussion

3.1. Structure of highly fluorinated graphite samples

Composition and X-ray diffraction data of C_xF samples are summarized in Table 1. The C/F ratio was in the range of 1.9–1.1, decreasing with increasing fluorine pressure and it was usually the lowest by the use of $KAgF_4$ as a fluorinating agent. Hydrogen (H) was detected in some samples by elemental analysis, mainly existing as HF in the samples. As shown by IR spectra later, all the samples contained small amounts of HF. Fluorination of graphite by fluorine gas in

Table 1
X-ray diffraction data and composition of C_xF samples prepared by high oxidation state complex fluorides and elemental fluorine in anhydrous HF at room temperature

Sample	Composition of H[a] (wt.%)		F_2 ($\times 10^5$ Pa)	Fluoride	X-ray diffraction data		
					Stage[b]	I_c (nm)	a_0 (nm)
1	$C_{1.7}F$	0.93	5.9	K_2PdF_6	1	0.629	0.245
2	$C_{1.6}F$	0.80	5.9	K_2PdF_6	1	0.582	0.246
					(2)	0.925	
3	$C_{1.9}F$	0.49	7.9	K_2MnF_6	1	0.599, 0.571	0.245
4	$C_{1.7}F$	0.75	7.9	K_2MnF_6	1	0.597	0.246
5[c]	$C_{1.2}F$	0.87	7.9	K_2NiF_6	1	0.644	
					(2)	0.933	0.246
					(3)	1.231	
6[d]	$C_{1.5}F$	0	7.9	K_2NiF_6	1	0.673	
					(2)	0.921	0.245
					(3)	1.226	
7[c,d]	$C_{1.6}F$	0	11.8	K_2NiF_6	1	0.647	0.247
8[d]	$C_{1.6}F$	0	11.8	K_2NiF_6	1	0.680	0.247
9[c]	$C_{1.1}F$	0.54	11.8	K_2NiF_6	1	0.639	
					(2)	0.942	0.247
					(3)	1.240	
10[c,d]	$C_{1.3}F$	0	11.8	$KAgF_4$	1	0.626	0.247
11[c,d]	$C_{1.4}F$	0	11.8	$KAgF_4$	1	0.628	0.248

[a] H detected by elemental analysis.
[b] ( ) minor phase.
[c] Ref. [14].
[d] Ref. [15].

aHF usually yields C_xF with a high fluorine content. The maximum C/F is approximately 2 [3–5]. The use of high oxidation state complex fluorides and fluorine gas under pressure provides highly fluorinated graphite with C/F ratio less than 2. All the prepared samples were composed of stage 1 structure though some of them contained stages 2 and 3 phases as minor components. The lattice parameter along *a-axis*, a_0 increased from 0.245 to 0.248 nm with increasing fluorine content, which means that average C–C bond length of graphene layer is lengthened with increase in the fluorine content. The formation of semi-ionic C–F bond at stage 1 causes the localization of electrons and may slightly change the sp^2 nature of graphene layers. It is thought that stage 1 C_xF with a composition of $\sim C_2F$ keeps planar (sp^2) graphene layers. However, the increase in the C–C bond length and slight puckering of graphene layers may occur in a highly fluorinated phase in which the fluorine content is higher than C_2F (C_2F–C_1F).

IR absorption spectra are shown in Fig. 1, and the assignment, C–C bond of graphene layers and possible C_xF phases are summarized in Table 2. The IR absorption spectra varied with increasing fluorine content. The absorptions observed at 1084 cm^{-1} and in the range of 1123–1134 cm^{-1} are assigned to the stretching vibration of semi-ionic C–F bond [5]. As the vibration energy is increased with increasing fluorine content, the absorption at 1084 cm^{-1} and those between 1123 and 1134 cm^{-1} with semi-ionic nature may be due to stage 1 C_3F and C_2F phases with sp^2 graphene layers, respectively, in comparison with the composition listed in Table 1. The absorptions at 1225 and 1230 cm^{-1} are due to C–F stretching vibration of covalent C–F bond with sp^3 hybridized orbital, being observed for graphite fluoride $(CF)_n$ [23,24]. A

Table 2
IR absorption peaks and assignments for C_xF samples

Absorption peak (cm^{-1}) of samples[a]					Assignment	Graphene layer	Possible C_xF phase
4	5	7	9	11			
1084	–	–	–	–	Semi-ionic C–F	sp^2	C_3F
1123	1125	1126	1131	1134	Semi-ionic C–F	sp^2	C_2F
–	–	–	1196	1196	Nearly covalent C–F	sp^2–sp^3	C_1F
1225	1225	1225	1230	1230	Covalent C–F	sp^3	$(CF)_n$
1257	1250	1257	1256	1256		sp^2	
1524	1524	1525	1524	1523		sp^2	
1570	1575	1570	–	–	A_{2u}	sp^2	

[a] Sample number is the same as given in Table 1.

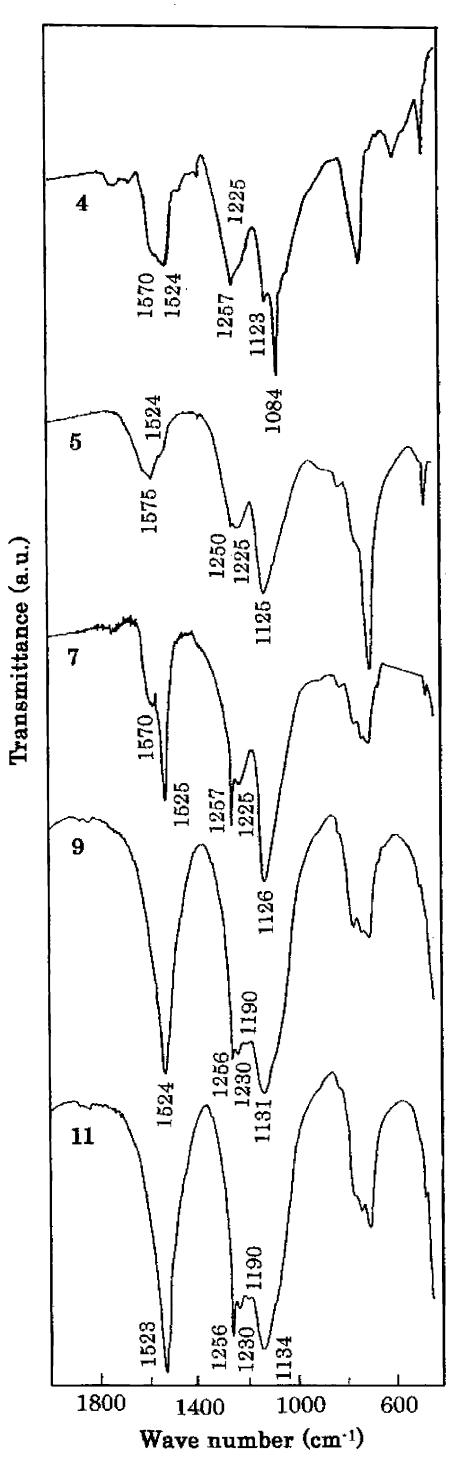

Fig. 1. IR absorption spectra of C_xF samples (4, 5, 7, 9 and 11 in the figure: sample numbers in Table 1).

new absorption was found at 1196 cm^{-1} between the above two absorptions. This may be assigned to the stretching vibration of nearly covalent C–F bond in somewhat puckered graphene layers, the composition of which may be C_1F. It was recently reported that the absorptions observed in the range of 1250–1257 cm^{-1} were due to C–C stretching in sp^2 graphene layers of C_xF containing HF [6]. This absorption disappeared and a new absorption appeared at 1220 cm^{-1} when HF was completely removed from C_xF [6]. It suggests that complete desolvation of HF from C_xF gives rise to the puckering of graphene layers by shortening the C–F bond length, that is, the formation of graphite fluoride $(CF)_n$ with puckered sp^3 graphene layers. The absorptions between 1250 and 1257 cm^{-1} thus show that all the C_xF samples in Table 1 contain trace amounts of HF. In addition to above absorptions, two absorptions were observed in the range of 1570–1575 cm^{-1} and 1523–1525 cm^{-1}. The absorptions observed at 1570 and 1575 cm^{-1} are located at slightly lower wave numbers than that of graphite, 1580 cm^{-1}, being attributed to A_{2u} mode indicating C–C stretching of graphene layers [25,26]. Since the absorptions have slightly weaker vibration energies than that of graphite itself, they may be derived of C_xF phase with relatively smaller amount of fluorine from C_3F to C_2F. The absorptions at 1523–1525 cm^{-1} possess more weaker vibration energies corresponding to longer C–C bond length in sp^2 graphene layers, probably arising from C_xF phase with a higher fluorine content, that is, $x \approx 2$.

The highly fluorinated graphite is composed of several different phases as shown in Table 2. The composition of stage 1 C_xF samples is normally in the range of C_4F to C_2F when they are prepared at room temperature by gas/solid reaction or in aHF using fluorine gas [1,2]. The highest fluorine content is obtained in the C_xF prepared in aHF [3–7,14]. In the present study, the C_xF with higher fluorine content than C_2F was prepared by the fluorination using high oxidation state transition metal complex fluorides and elemental fluorine under pressure. Since graphite is a polycrystal, the fluorination degree may not be uniform in crystallites constituting a graphite particle. If C_3F or C_2F phase with planar graphene layers exists in the same crystallite with graphite fluoride $(CF)_n$ having puckered graphene layers, such a structure may be unstable due to a high structural strain. Graphite fluoride $(CF)_n$ and stage 1 C_xF are, however, both stable compounds even at high temperatures [1,2,27]. This suggests that highly fluorinated phases having planar and puckered graphene layers normally consist of different crystallites from each other though some transient states from sp^2 to sp^3 structure may exist. The lattice parameter, a_0, values given in Table 1 were obtained by X-ray diffraction as average values for several different phases in C_xF samples.

3.2. Electrochemical behavior of highly fluorinated graphite

Typical discharge curves of C_xF samples are shown in Figs. 2–4. Fig. 2 demonstrates the discharge curves of samples 2, 3 and 4 prepared using K_2PdF_6 or K_2MnF_6 and elemental fluorine at a current density of 10 mA/g. The discharge potentials were 3.1 V versus Li/Li^+ at the beginning of discharge, gradually decreasing with progress in the discharge. Discharge capacities at cut-off potential of

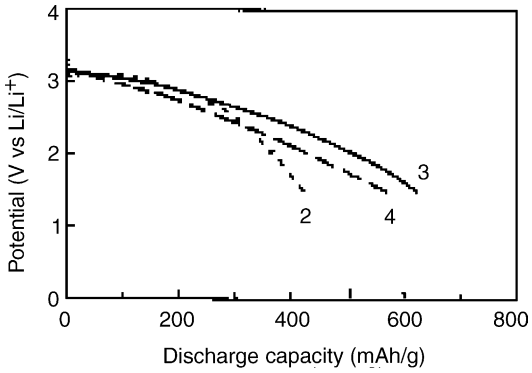

Fig. 2. Discharge curves of C_xF samples, obtained at 10 mA/g in 1 mol/dm^3 $LiClO_4$–PC at 25 °C (2, 3 and 4 in the figure: sample numbers in Table 1).

1.5 V were 420, 620 and 570 mAh/g for samples 2, 3 and 4, respectively. In these samples, H was detected by elemental analysis, indicating the cointercalation of HF molecules in graphite. The discharge capacity was reduced as the amount of cointercalated HF was increased. Although the content of H in sample 2 determined by chemical analysis was not the highest, sample 2 may have contained larger amount of HF than samples 1, 3 and 4 because stage 2 phase was present (Table 1). In stage 2 phase, intercalated fluorine atoms exist mainly as $HF_2^{\delta-}$ because stage 2 and higher stages of C_xF have nearly ionic C–F bond [1,2]. It seems that a part of intercalated fluorine atoms exists as $HF_2^{\delta-}$ even in stage 1 phase because a trace amount of HF was contained in all the samples as already shown by IR spectra. Fig. 3 shows the discharge curves of samples 7 and 9 prepared by K_2NiF_6 and elemental fluorine at a current density of 10 mA/g. The discharge capacities were 423 and 260 mAh/g at cut-off potential of 1.5 V for samples 7 and 9, respectively. The result shows that the capacity was much smaller for sample 9 containing the larger amount of HF and stage 2 and 3 phases. For the C_xF samples prepared by K_2NiF_6 and elemental fluorine, those containing smaller amounts of HF than sample 9 gave the larger discharge capacities of 422–580 mAh/g

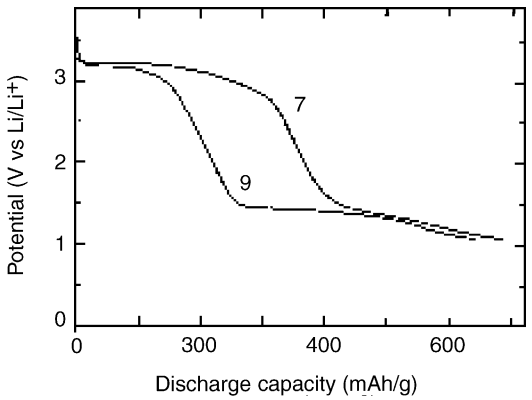

Fig. 3. Discharge curves of C_xF samples, obtained at 10 mA/g in 1 mol/dm^3 $LiClO_4$–PC at 25 °C (7 and 9 in the figure: sample numbers in Table 1).

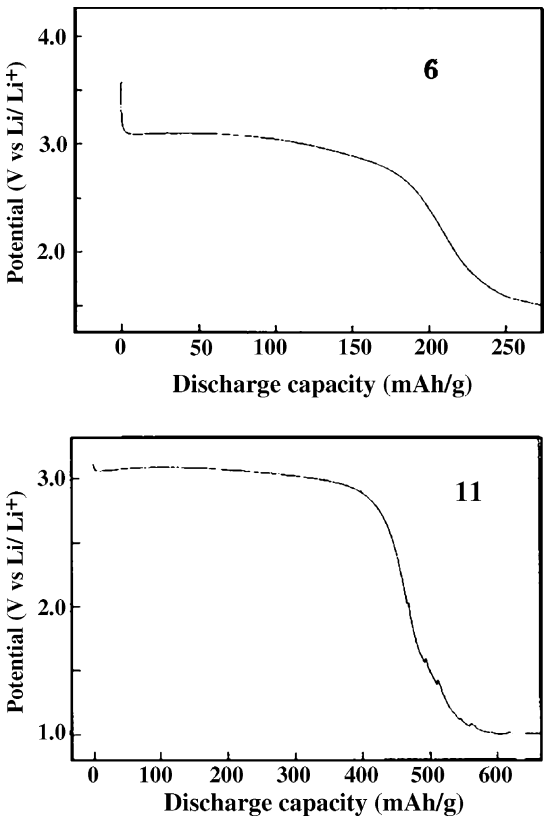

Fig. 4. Discharge curves of C_xF samples, obtained at 35 mA/g (sample 6) and 40 mA/g (sample 11) in 1 mol/dm^3 $LiClO_4$–PC at 25 °C (6 and 11 in the figure: sample numbers in Table 1).

at cut-off potential of 1.5 V [14]. The discharge at higher current densities gave the similar result as shown in Fig. 4. Samples 6 and 11 exhibited very different capacities, 275 and 500 mAh/g at current densities of 35 and 40 mA/g at cut-off potential of 1.5 V, respectively. The same samples had 460 and 515 mAh/g, respectively when they were discharged at 10 mA/g [14]. H was not detected by elemental analysis for these samples, however, both of them contained trace amounts of HF as shown by IR spectra. Sample 6 seems to have contained a larger amount of HF than sample 11 because stage 2 and 3 phases were mixed in sample 6 as minor components. Fluorination of graphite by $KAgF_4$ and elemental fluorine yields highly fluorinated C_xF such as samples 10 and 11 having high fluorine contents with $x < 1.5$. Sample 11 demonstrated the flat discharge potential at ca. 3 V until about 400 mAh/g and the capacity was not largely decreased by the increase in the current density. The discharge capacities of samples 6, 7 and 8, obtained at a low current density of 10 mA/g and at cut-off potential of 1.0 V reached 93–96% of their theoretical values calculated from the composition (Fig. 3 and Ref. [14]). This shows that cointercalation of HF in C_xF is responsible for the decrease in the discharge capacities at both low and high current densities (10 and 35–40 mA/g, respectively).

The discharge capacities and potential profiles would be governed by several factors such as fluorine content, amount

of cointercalated HF and coexistence of stage 2 and 3 phases. C_xF with a high fluorine content generally shows a large discharge capacity. In the present study, C_xF samples possessed three kinds of C–F bonds, that is, semi-ionic, covalent and nearly ionic C–F bonds with composition between C_2F and C_1F. Discharge reaction of graphite fluoride $(CF)_n$ with covalent C–F bond proceeds with formation of an intermediate discharge product containing C, F^-, Li^+ and solvent molecules, which is metastable, determining an OCV of $Li/(CF)_n$ cell [1,28–30]. The intermediate discharge product finally decomposes to carbon (C), LiF and solvent molecules (S).

$$(CF)_n + nLi^+ \cdot S + ne^- \rightarrow nC \cdots F^- \cdots Li^+ \cdots S \rightarrow nC + nLiF + nS \quad (3)$$

The discharge reaction of C_xF would be basically similar to that of graphite fluoride, however, the reaction rate changes depending on whether HF coexists or not.

$$C_xF + Li^+ \cdot S + e^- \rightarrow C_x \cdots F^- \cdots Li^+ \cdots S \rightarrow xC + LiF + S \quad \text{(fast)} \quad (4)$$

$$C_xF + HF + Li^+ \cdot S + e^- \rightarrow C_x \cdots F^- \cdots HF \cdots Li^+ \cdots S \rightarrow xC + LiHF_2 + S \quad \text{(slow)} \quad (5)$$

$$C_x{}^{\delta+}HF_2{}^{\delta-} + Li^+ \cdot S + e^- \rightarrow C_x \cdots F^- \cdots HF \cdots Li^+ \cdots S \rightarrow xC + LiHF_2 + S \quad \text{(slow)} \quad (6)$$

The discharge capacities strongly depended on the amounts of cointercalated HF and coexistence of stage 2 and 3 phases. The C–F bonding in stage 2 and 3 phases is nearly ionic, and main intercalated fluorine species are mobile $HF_2{}^{\delta-}$. All the samples contained small amounts of HF as shown by IR spectra even in case that H was not detected by elemental analysis. The cointercalation of HF in stage 1 phase also suggests the coexistence of a trace amount of $HF_2{}^{\delta-}$. The discharge capacity was larger in the stage 1 C_xF samples containing the smaller amount of HF without stage 2 and 3 phases as already shown. If HF does not coexist in C_xF, the intermediate discharge product, $C_x \cdots F^- \cdots Li^+ \cdots S$ would smoothly decompose to carbon, LiF and solvent molecules because of a strong interaction between F^- and Li^+ due to a large surface charge of a small fluoride ion (Eq. (4)). Therefore, the discharge reaction may proceed well without potential decrease for C_xF containing less amount of cointercalated HF. On the other hand, when HF is present in C_xF phase, decomposition of the intermediate discharge product, $C_x \cdots F^- \cdots HF \cdots Li^+ \cdots S$ may be slow because of a weak interaction between $HF_2{}^-$ and Li^+ due to a small surface charge of a large $HF_2{}^-$ anion (Eq. (5)). Slow decomposition of the intermediate discharge product would give rise to the gradual decrease in the discharge potential, leading to the reduction of the discharge capacity. This is more evident at a high current density (sample 6 in Fig. 4). The discharge potentials were about 3 V versus Li/Li^+ at the beginning of discharge, but decreased to a plateau at ca. 1.5 V with progress in the discharge in such samples as 6, 7 and 9 (Figs. 3 and 4) in which $HF_2{}^{\delta-}$ would have coexisted. These results suggest that the discharge potential of covalently and semi-ionically bonded fluorine atoms is ca. 3 V (Eqs. (4) and (5)) and that for fluorine atom in $HF_2{}^{\delta-}$ is ca. 1.5 V versus Li/Li^+ (Eq. (6)). Therefore, complete formation of stage 1 phase with semi-ionic or covalent C–F bonds and thorough removal of HF from prepared samples are needed to obtain a flat discharge potential and high capacity. For this purpose, $KAgF_4$ seems the best fluorinating agent.

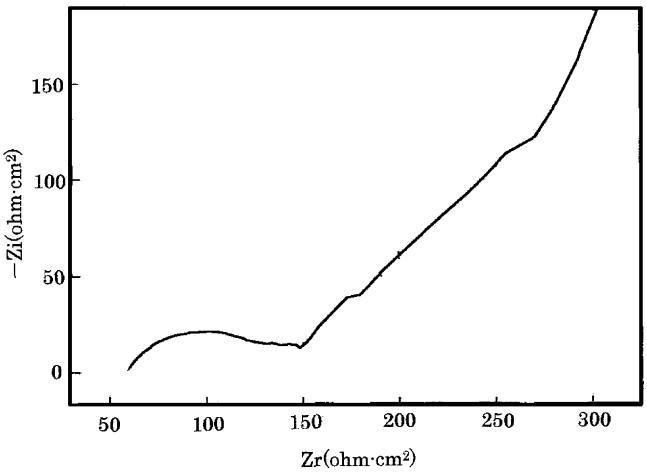

Fig. 5. Nyquist diagram for sample 6 in Table 1, obtained after 60 min discharge at 35 mA/g in 1 mol/dm^3 $LiClO_4$–PC at 25 °C.

The kinetic characteristics of lithium insertion were deduced from *ac* impedance measurements. Fig. 5 shows a typical Nyquist diagram, obtained for sample 6 after 60 min discharge at 35 mA/g (OCV: 3.78 V versus Li/Li^+). The similar results were obtained for samples 8, 10 and 11. The electrochemical impedance response of the system was analyzed using a Randles equivalent circuit comprising the Ohmic drop in the electrolyte (R_e), the charge transfer resistance for the half-reaction corresponding to the reduction of C_xF (R_t), the double layer capacitance (C_{dl}), and the Warburg impedance (Z_w). At high frequency, the semi-circle in the Nyquist diagram is related to the charge transfer phenomenon. At low frequency, a straight line showing a 45° angle against the real axis was obtained. It corresponds to the Warburg impedance (semi-infinite diffusion). A second straight line showing a higher slope was observed at lower frequencies due to the finite thickness of the electrode which induces a finite length diffusion process. For ideal cases, the slope of this branch is infinite. Ho et al. [21] showed that the chemical diffusion coefficient of lithium ion, $D_{Li}{}^+$ may be obtained by solving Fick's law with appropriate initial and boundary conditions. They showed that the

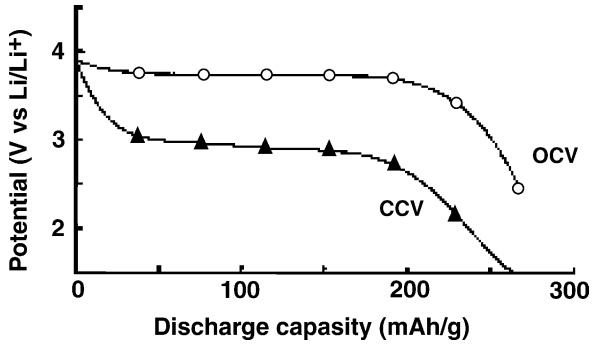

Fig. 6. OCV and CCV for C_xF (sample 6 in Table 1) as a function of discharge capacity.

Warburg impedance has a constant phase angle of 45° and is expressed as:

$$Z_w = A_\omega(1 - j)\omega^{-1/2} \quad (7)$$

where ω is the angular frequency of the signal. The coefficient A_ω is given by:

$$A_\omega = V_m \frac{(dE/dy)}{2^{1/2}} nF(D_{Li}{}^+)^{1/2} S \quad (8)$$

where V_m is the molar volume of the host structure, y is the discharge ratio, dE/dy is the slope of OCV versus y values, n is the number of exchanged electron during the electrochemical reaction, F is the Faraday constant, $D_{Li}{}^+$ is the chemical diffusion coefficient of Li^+, S is the geometric surface area of the electrode. For example, the CCVs and OCVs obtained for sample 6 are presented in Fig. 6.

The chemical diffusion coefficients of Li^+ were deduced by the exploitation of the Warburg impedance in the low frequency region showing a 45° angle against the real axis using Eq. (8). The data are listed in Table 3. For all samples, the diffusion coefficients were nearly constant irrespective of the discharge ratios. Table 3 indicates that samples 6 and 8 with lower fluorine contents had higher diffusion coefficients than samples 10 and 11. H was not detected in these four samples by elemental analysis. However, samples 6 and 8 may have contained larger amounts of HF than samples 10 and 11 because sample 6 had stage 2 and 3 phases and discharge capacities of samples 6 and 8 (275 and 175 mAh/g, respectively) were much smaller than those of samples 10 and 11 (440 and 500 mAh/g, respectively), though the fluorine contents were somewhat higher in samples 10 and 11 than samples 6 and 8. Large $HF_2{}^-$ anion would have a weaker interaction with Li^+ cation than small F^- anion. Therefore, $HF_2{}^-$ and Li^+ would be mobile in the intermediate discharge product. This may be the reason why the larger diffusion coefficients were obtained for samples 6 and 8 than samples 10 and 11. The exploitation of the impedance diagrams leads to the determination of the charge transfer resistance, R_t. It was reported that charge transfer resistance of C_xF prepared at room temperature using elemental fluorine with HF and IF_5 was about half of the value for $(CF)_n$ with covalent bond [11]. Table 3 also shows the values obtained in the present study at discharge ratio, $y = 0.3$. The charge transfer resistances were in the range of 73–93 $\Omega\,cm^2$.

Table 3
Chemical diffusion coefficients of lithium ion

Sample[a]	F/C ratio	R_t[b] ($\Omega\,cm^2$)	$D_{Li}{}^+$ ($\times 10^{-12}\,cm^2/s$)
6	0.65	82	13
8	0.62	84	11
10	0.80	93	4.4
11	0.73	73	5.7

[a] Sample number is the same as given in Table 1.
[b] Charge transfer resistance obtained at the discharge ratio, $y = 0.3$.

4. Conclusion

Highly fluorinated graphite was prepared at room temperature using high oxidation state transition metal complex fluoride and elemental fluorine under pressure in aHF. The composition of the products was between C_2F and C_1F. IR absorption spectra revealed that stage 1 phase of C_xF was composed of several different phases having planar (sp^2) and puckered (sp^3) graphene layers with semi-ionic and covalent C–F bonds. Discharge potentials of C_xF phases with semi-ionic and covalent C–F bonds were about 3 V at current densities of 10, 35 and 40 mA/g, gradually decreasing with discharge for the samples containing relatively larger amounts of HF. Discharge potential of fluorine atom in $HF_2{}^{\delta-}$ may be ca. 1.5 V versus Li/Li^+. Discharge capacities were in the range of 175 and 620 mAh/g, being also less for the samples with relatively larger amounts of HF. The decrease in the discharge potential and capacity may be due to slow decomposition of the intermediate discharge product, $C_x \cdots F^- \cdots HF \cdots Li^+ \cdots S$ to carbon, $LiHF_2$ and solvent molecules. Chemical diffusion coefficients of Li^+ ion obtained by impedance measurement were one order higher in C_xF samples with relatively larger amounts of HF.

Acknowledgements

The present study was partly supported by a grant of the Frontier Research Project “Materials for the 21st Century – Materials Development for Environment, Energy and Information” (for 2002–2006 fiscal years) from Ministry of Education, Culture, Sports, Science and Technology of Japan, and also by the Research Project P1-0045 Inorganic Chemistry and Technology of the Ministry of Education, Science and Sport of the Republic of Slovenia.

References

[1] T. Nakajima, N. Watanabe, Graphite Fluorides and Carbon-Fluorine Compounds, CRC Press, Boca Raton, FL, 1991 (and references therein).

[2] T. Nakajima, Synthesis, Structure and physicochemical properties of fluorine–graphite intercalation compounds, in: T. Nakajima (Ed.), Fluorine–Carbon and Fluoride–Carbon Materials, Marcel Dekker, New York, NY, 1995 (and references therein).
[3] T. Mallouk, N. Bartlett, J. Chem. Soc. Chem. Commun. (1983) 103.
[4] R. Hagiwara, M. Lerner, N. Bartlett, J. Chem. Soc. Chem. Commun. (1989) 573.
[5] T. Mallouk, B.L. Hawkins, M.P. Conard, G.E. Zilm, K. Maciel, N. Bartlett, Philos. Trans. R. Soc. Lond. Ser. A 314 (1985) 179.
[6] Y. Sato, T. Kume, R. Hagiwara, Y. Ito, Carbon 41 (2003) 351.
[7] Y. Sato, S. Shiraishi, Z. Mazej, R. Hagiwara, Y. Ito, Carbon 41 (2003) 1971.
[8] A. Hamwi, M. Daoud, J.C. Cousseins, Synth. Metals 30 (1989) 23.
[9] A. Hamwi, J. Phys. Chem. Solids 57 (1996) 677.
[10] P. Hany, R. Yazami, A. Hamwi, J. Power Sources 68 (1997) 708.
[11] R. Yazami, P. Hany, P. Masset, A. Hamwi, Mol. Cryst. Liq. Cryst. 310 (1998) 397.
[12] T. Nakajima, Y. Matsuo, B. Žemva, A. Jesih, Carbon 34 (1996) 1595.
[13] J.P. Lemmon, M.M. Lerner, Carbon 31 (1993) 437.
[14] T. Nakajima, M. Koh, V. Gupta, B. Žemva, K. Lutar, Electrochim. Acta 45 (2000) 1655.
[15] V. Gupta, T. Nakajima, Y. Ohzawa, B. Žemva, Mol. Cryst. Liq. Cryst. 386 (2002) 25.
[16] T. Nakajima, M. Kawaguchi, N. Watanabe, Electrochim. Acta 27 (1982) 1535.
[17] R. Hagiwara, M. Lerner, N. Bartlett, T. Nakajima, J. Electrochem. Soc. 135 (1988) 2393.
[18] Z. Mazej, J. Fluorine Chem. 114 (2002) 75.
[19] Z. Mazej, K. Lutar, J. Fluorine Chem. 107 (2001) 63.
[20] T. Nakajima, M. Koh, R.N. Singh, M. Shimada, Electrochim. Acta 44 (1999) 2879.
[21] C. Ho, I.D. Raistrick, R.A. Huggins, J. Electrochem. Soc. 127 (1980) 343.
[22] H. Groult, T. Nakajima, N. Kumagai, D. Devilliers, J. Power Sources 62 (1996) 107.
[23] V.K. Mahajan, R.B. Badachhape, J.L. Margrave, Inorg. Nucl. Chem. Lett. 10 (1974) 1103.
[24] Y. Kita, N. Watanabe, Y. Fujii, J. Am. Chem. Soc. 101 (1979) 3832.
[25] F. Tuinstra, J.L. Koenig, J. Chem. Phys. 53 (1970) 1126.
[26] D.S. Knight, W.B. White, J. Mater. Res. 4 (1989) 385.
[27] Y. Sato, R. Hagiwara, Y. Ito, J. Fluorine Chem. 110 (2001) 31.
[28] N. Watanabe, R. Hagiwara, T. Nakajima, H. Touhara, K. Ueno, Electrochim. Acta 27 (1982) 1615.
[29] H. Touhara, H. Fujimoto, N. Watanabe, A. Tressaud, Solid State Ionics 14 (1984) 163.
[30] N. Watanabe, T. Nakajima, R. Hagiwara, J. Power Sources 20 (1987) 87.